Autonomous Transportation and Deployment with Aerial Robots for Search and Rescue Missions

Markus Bernard
Technische Universität Berlin, Einsteinufer 17, 10587 Berlin, Germany
e-mail: markus.bernard@gmx.de
Konstantin Kondak
Institute of Robotics and Mechatronics, DLR (German Aerospace Center), Muenchner Strasse 20, 82234 Oberpfaffenhoffen-Wessling, Germany
e-mail: Konstantin.Kondak@dlr.de
Ivan Maza and Anibal Ollero*
Robotics, Vision and Control Group, Universidad de Sevilla, 41092 Seville, Spain
e-mail: imaza@us.es, aollero@cartuja.us.es

Received 26 November 2010; accepted 20 May 2011

It is generally accepted that systems composed of multiple aerial robots with autonomous cooperation capabilities can assist responders in many search and rescue (SAR) scenarios. In most of the previous research work, the aerial robots are mainly considered as platforms for environmental sensing and have not been used to assist victims. In this paper, outdoor field experiments of transportation and accurate deployment of loads with single/multiple autonomous aerial vehicles are presented. This is a novel feature that opens the possibility to use aerial robots to assist victims during rescue phase operations. Accuracy in the deployment location is a critical issue in SAR scenarios in which injured people may have very limited mobility. The presented system is composed of up to three small-size helicopters and features cooperative sensing, using several different sensor types. The system supports several forms of cooperative actuation as well, ranging from the cooperative deployment of small sensors/objects to the coupled transportation of slung loads. The complete system is described, outlining the hardware and software framework used, as well as the approaches for modeling and control used. Additionally, the results of several flight field experiments are presented, including a description of the worldwide first successful autonomous load transportation experiment, using three coupled small-size helicopters (conducted in December 2007). During these experiments strong, steady winds and wind gusts were present. Various solutions and lessons learned from the design and operation of the system are also provided.

1. INTRODUCTION

Search and rescue (SAR) takes many forms, each with its own unique risks and dangers to victim and responder (Murphy et al., 2008). Urban SAR (USAR) has been the most studied form of SAR in the robotics research community (Arai, Tanaka, Hirose, Kuwahara, & Tsukui, 2008; Birk & Carpin, 2006; Gage, Murphy, Rasmussen, & Minten, 2004; Micire, 2008; Murphy & Stover, 2008; Poppinga, Birk, & Pathak, 2008) and has become familiar as recent natural and man-made disasters have made the news the world over. On the opposite end of the spectrum, wilderness SAR (WiSAR) often involves only a few victims with a large geographic search region (Goodrich et al., 2008).

Systems composed of multiple robots with autonomous cooperation capabilities can assist responders in both USAR and WiSAR scenarios. There are related projects dealing with multirobot teams in emergency situations such as the EMBER CMU project, which aims to assist first responders by providing tracking information and coordination abilities. In EMBER, range information is used for searching and tracking of mobile targets, using multiple robots (Hollinger, Singh, Djugash, & Kehagias, 2009). Multiagent (combined ground and air) tasking also has been demonstrated recently (Hsieh, 2007; Hsieh, Cowley, Kumar, & Taylor, 2008).

It is noteworthy that in most of the research work, aerial robots are mainly considered as platforms for environmental sensing; they are not used to assist victims during rescue phase operations. The closest experimental approach to this concept found in the literature was the use of

Multimedia files may be found in the online version of this article.
*Also with the Center for Advanced Aerospace Technologies (CATEC), Parque Tecnológico y Aeronáutico de Andalucía, C. Wilbur y Orville Wright 17-19-21, 41309 La Rinconada, Spain.

autonomous helicopters for the deployment and repair of a wireless sensor network (Corke et al., 2004a, 2004b).

In anticipation of the results presented in this paper, it is stated that the transportation and accurate deployment of loads with single/multiple autonomous aerial vehicles have been successfully demonstrated in outdoor field experiments. As was mentioned above, this is a novel feature that opens the possibility to use aerial robots to assist victims during rescue phase operations. For instance, it could be possible to command such a transportation system to deploy medical kits, oxygen masks, satellite phones, etc., in places very close to the victims. Accuracy in the deployment location is a critical issue in SAR scenarios when injured people may have very limited mobility. The system can be very useful in flooding disaster scenarios in which hundreds of people are isolated on the roofs of their houses.

The joint transportation of a load by several ground robots has been a subject of active research and development for many years. The coordinated control of the motion of the vehicles needs to consider the forces involved. Thus, each robot could be controlled around a common compliance center attached to the transported object. Assuming that each robot holds the object firmly, the trajectories of all the robots determine the trajectory of the object. Both centralized and decentralized compliant motion control algorithms have been proposed, including the consideration of nonholonomic constraints (Kosuge & Sato, 1999). The method has been implemented in an experimental system composed of three tracked mobile robots equipped with a force sensor. In Sugar and Kumar (1998) the decentralized control of cooperating mobile manipulators is studied, in which a designated lead robot is responsible for task planning. The control of each robot is decomposed (mechanically decoupled) into the control of the gross trajectory and the control of the grasp. The excessive forces due to robot positioning errors and odometry errors are accommodated by the compliant arms. In Borenstein (2000) the Omnimate system, which uses a compliant linkage platform between two differential-drive mobile robots, is presented. In Huntsberger et al. (2004) the distributed coordinated control of two rovers, carrying a 2.5-m-long mock-up of a photovoltaic tent is presented and demonstrated as an example of the CAMPOUT behavior-based control architecture.

The single-lift configuration, in which a long rope couples one helicopter and one load, is the only configuration commercially utilized for the transportation of slung loads. Several textbooks (see, for example, Wagtendonk, 2006) provide information about the correct attachment of the slung loads and important safety procedures. However, the manual maneuvering of a helicopter with an attached slung load is very difficult and requires a skillful and experienced pilot. In particular the active damping of load oscillations is a difficult task that most pilots avoid. Instead the pilots stabilize only the helicopter and wait for the load oscillation to die down. To support manual piloted slung-load operations, the iMAR GmbH and the German Aerospace Center DLR developed the "iSLD-IVC" (iMAR Slung Load Damping based on inertial stabilized vision control) system, which uses an artificial horizon instrument to guide the pilot. The authors are not aware of a completely autonomous system for full-size helicopters. The system presented in this work provides the full autonomous control of single-lift, slung-load configurations (based on small-size helicopters), including the active damping of load oscillations.

The joint transportation of a single load by means of several helicopters has also been proposed in the literature. In experiments with two manned, manually piloted helicopters, it was determined that the control of two coupled helicopters is a very challenging task that emphasizes the need for automatic helicopter stabilization. The motivation for using two or more small helicopters instead of one with bigger load capacity is as follows:

- In the case of real manned transport helicopters, the costs of two small helicopters are often less than for one with double-load capacity.
- Independent of the load capacity of the most advanced helicopters, there is always a task that requires more load capacity than provided by a single helicopter. In this case the control software allows the coupling of the existing helicopters, in order to form a system with sufficient load capacity.

In particular, research on lifting and transportation of loads by means of two helicopters (twin-lift, dual-lift) was presented in, e.g., Mittal, Prasad, and Schrage (1991) and Reynolds and Rodriguez (1992). This research has been done only in simulation. Experimental results with a team of aerial robots to manipulate and transport a payload in three dimensions via cables were recently presented (Michael, Fink, & Kumar, 2010). The authors propose two quality measures for motion plan design that minimize individual robot motion and maximize payload stability along the trajectory. However, field experiments involving the lifting and transportation of loads by means of autonomous aerial robots are not addressed in the literature.

In this paper, field experiments featuring the load transportation with one helicopter (single-lift) and three helicopters (multilift) are presented. Ciolani and Kanning (1992) identify in their work 12 typical slung-load configurations: three single-lift configurations, four single-lift configurations using a twin-rotor helicopter, three dual-lift configurations, and two multilift configurations. The orientation controller proposed in our paper features a measurement-based torque compensation and is applicable for single-, dual-, and multilift load transportation. Therefore, the theoretical results of this work are applicable to all configurations presented by Ciolani and Kanning, except

for the twin-rotor-helicopter configurations, which require an adaptation of the helicopter model used.

The described automatic control system allows the use of one or multiple small-size helicopters for slung-load transportation. The number of helicopters is configurable depending their capabilities and the properties of the load to be transported.

The paper is structured as follows. First, the physical system is described in Section 2. Then Section 3 is devoted to the transportation of a single load by means of multiple coupled helicopters. Section 4 presents field experiments with one and three helicopters. Finally, the lessons learned from the field experiments and the conclusions close the paper.

2. UNMANNED AERIAL VEHICLE DESCRIPTION

In Figure 1 one of the TUB-H unmanned aerial vehicles (UAVs), developed by the Technische Universität Berlin (TUB) and used for the slung-load transportation experiments is shown. The UAVs are based on commercially available small-size helicopters. The helicopters have a rotor diameter of 1.8 m and a main rotor speed of approximate 1,300 rpm and are powered by a 1.8-kW, two-stroke engine. The UAVs can carry about 1.5 kg of additional payload, and the weight of the UAV itself is 12.5 kg. The different components necessary to achieve autonomous flight capabilities are mounted to the helicopters, using a frame composed of strut profiles. Through the use of these profiles, the location of hardware components can be altered and new hardware can be installed easily. This allows quick reconfiguration of the UAVs for different applications, easy replacement of defective hardware, and alteration of the positions of different components to adjust the UAV's center of gravity. The components necessary for autonomous operation are shown in Figure 1: a GPS, an inertial measurement unit (IMU), a control computer, and a communication link. Owing to the strong magnetic field of the engine, a magnetic field sensor is mounted on the tail.

The various payloads necessary for the different experiments were mounted to the same frame, composed of strut profiles, which was used to attach the components necessary for autonomous flight. The following payloads were used during the different missions:

- Fixed visual and infrared cameras.
- A *deployment device* (DD) developed by the TUB (see Figure 2). The functionality of the device is similar to the functioning of candy bar vending machines: A metal grommet is attached to a small object (the payload) through a short wire. This grommet is attached to the right end of a steel spring. A clockwise rotation of the spring moves the grommet (and the object) further onto the spring. This procedure allows the attachment of several small objects to the helicopter. During the dropping maneuver the spring rotates counterclockwise until the rightmost grommet is moved beyond the end of the spring and the object is released.
- The *load transportation devices* (LTDs), which are specially designed for the transportation of slung loads using one or more UAVs. The LTD (see Figure 3) is composed of a two-axis cardan joint with two magnetic encoders attached to each axis. After the joint, a force sensor and the release mechanism for the rope are attached. The release mechanism is composed of a bolt, which is inserted into a tube. The bolt is fixed in the tube through a pin, which can be pulled out by a small motor to release the load. The release mechanism can be used for emergency decoupling of the load from the UAV (and for the decoupling from the remaining UAVs), but also to release the load after successful transportation. The magnetic encoders allow the measurement of the rope orientation relative to the UAV fuselage. With this information and the measured rope force, it is possible to calculate the torques and forces imposed on the UAV

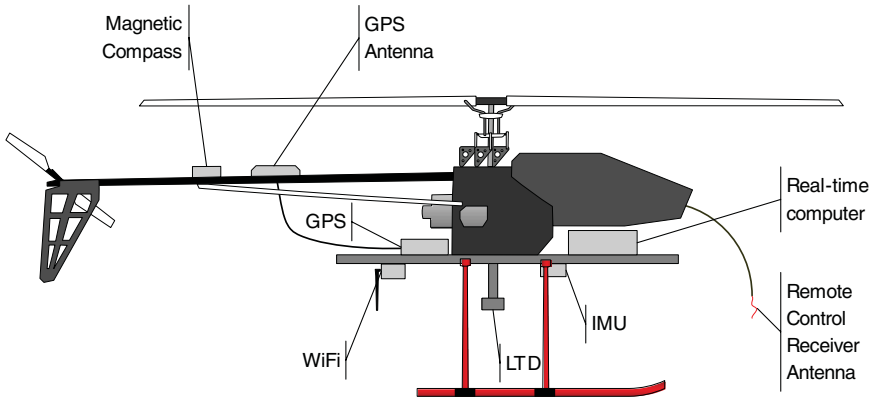

Figure 1. TUB-H UAV developed by the TUB used in the field experiments.

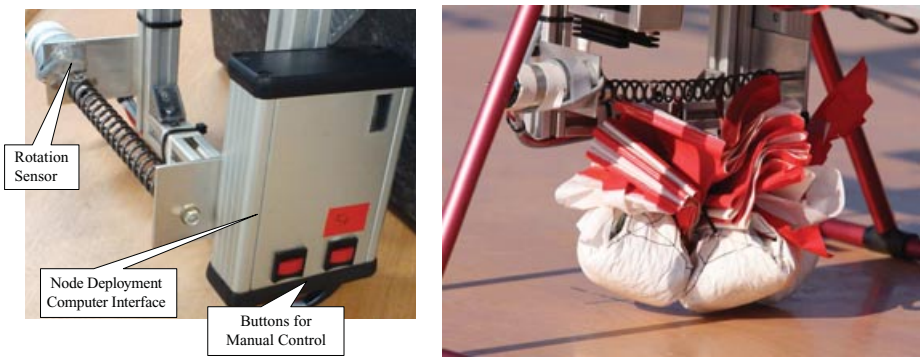

(a) Components of the DD

(b) DD loaded with several small objects (sensors in this photograph)

Figure 2. Detailed view of the DD developed by the TUB. It was used onboard the helicopter for missions that required the autonomous deployment of objects (sensors) in a given place.

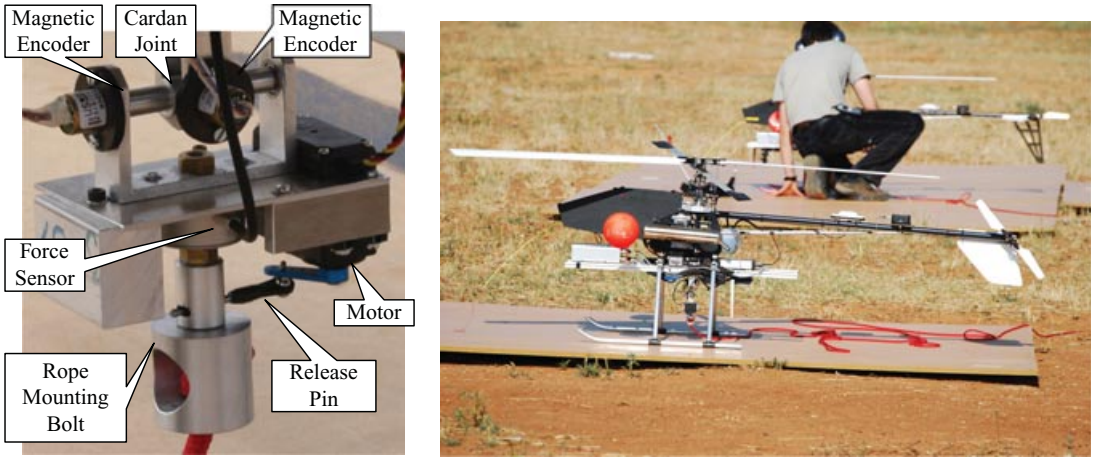

(a) Components of the LTD

(b) TUB-H helicopter equipped with the LTD on the landing pad

Figure 3. Detail of the LTD developed by the TUB. It was used onboard the helicopter for missions that required the autonomous transportation of objects to a given location.

through the load (and/or the other coupled UAVs). This information is used in the feedback loop of compensator block C; see Section 3.3.

In Figure 4 the concept of the software system running on the UAV board computers is shown. The real-time base system is composed of multiple separate modules, which are connected by an Interprocess Communication and System Management Library (ICSML). The ICSML offers, among other features, convenient interprocess communication methods, using a shared memory design and an event system for interprocess notifications (e.g., on the change of shared memory variables). The driver modules are used to communicate with the peripheral devices of the UAV, such as the compass, IMU, or GPS. The device-specific protocol is encapsulated in the driver process, and the sensor data are presented to the remaining system through the ICSML as generalized objects. The controller of the system was designed and tested in simulation using Matlab/Simulink. The real-time base system (RTBS) provides a generic wrapper module to embed C-code generated by Matlab/Simulink. This allows the fast implementation of new control algorithms and an error-free transition from Simulink models to real-time controller code. On the other hand, the executive layer module provides the basic functionality needed to integrate the UAV with the rest of the components of a SAR platform. This includes the commanding of the UAVs and reporting of the command execution progress and the UAV state. Additionally the executive layer module provides a certain level of hardware abstraction: The relative configuration of the UAVs during the load transportation is part of the control loop and should not

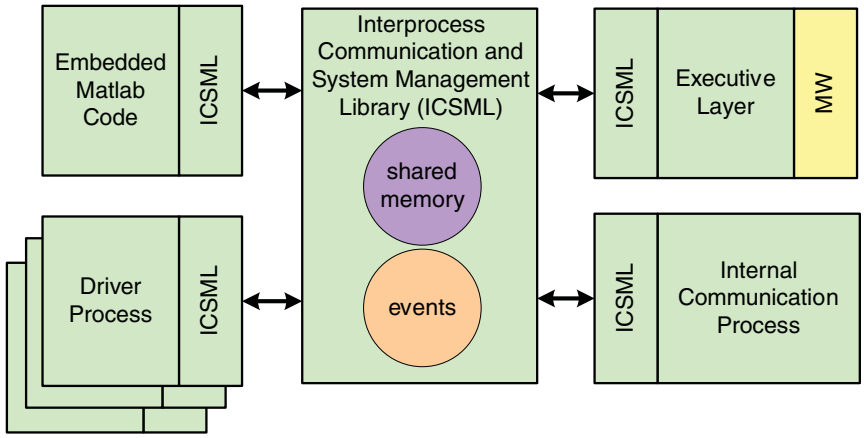

Figure 4. RTBS composed of multiple separate modules, which are connected by an ICSML.

be altered by the user of the platform (the coupled UAVs are presented as a single entity). This way the commanding interfaces for coupled and uncoupled UAVs are equal for both the user and the possible autonomous decision-making software of the SAR platform.

3. MULTI-UAV LOAD TRANSPORTATION AND DEPLOYMENT

The transportation of loads using only one UAV is strongly limited by the payload capacity of the UAV itself. Assuming the use of small-size UAVs, this constraint may prevent the transportation and deployment of loads required for a particular application (for example, heavy communication equipment or first aid supplies required for victims in SAR operations). The system designed allows the transportation of a single load by means of several helicopters. The number of helicopters is configurable, depending on the capabilities of the helicopters and the load to be transported.

3.1. Modeling

The model of a small-size helicopter is a key component for the behavior description of a system composed of one or several helicopters, which are coupled to a load by means of ropes. We use the model presented in our previous work (Kondak, Bernard, Losse, & Hommel, 2006; Kondak, Bernard, Meyer, & Hommel, 2007). A small-size model helicopter shows some specific effects that are not presented or are negligibly small in the case of the full-size helicopter and vice versa. For this reason, it is impossible to use the models derived for full-size helicopters, see e.g., Johnson (1980), without any adaptation. As was pointed out in our previous work, the main differences between model and full-size helicopters in respect to modeling and control are as follows:

- a higher main-rotor-to-fuselage-mass ratio
- a higher main rotor revolution speed (than for most full-size helicopters)
- a very stiff main rotor without flapping hinges (almost all purchasable model helicopters)

Owing to these differences, the inertial effects of the main rotor make a significant contribution to the rotational dynamics of the system and cannot be neglected. Therefore, the mechanical model should be considered as being composed of two rigid bodies: the main rotor and the fuselage. For the considered class of model helicopters, the dominant component is the main rotor and not the fuselage. Unfortunately, the main rotor is very often neglected in papers related to modeling and control of small-size helicopters and only one rigid body—the fuselage—is accounted for in the dynamic equations.

The complete model of a helicopter is composed of two main components: the mechanical model and the model for generation of aerodynamic forces and torques. From experimental results with helicopters we concluded that the generation of aerodynamic forces and torques, at least for the considered class of helicopters, can be approximated with simple algebraic relations (the corresponding time delay is approximated by a simple first-order delay). Therefore, the dynamics of one small-size helicopter or of a system composed of several coupled helicopters are mostly determined by its mechanical model. The lifting forces $\mathbf{F}_3^{\mathrm{MR}}$ and torques $\mathbf{T}_{1,2}^{\mathrm{MR}}$ generated by the main rotor of each helicopter (see Figure 5) and the forces $\mathbf{F}_2^{\mathrm{TR}}$ (not shown in Figure 5) generated by the tail rotors are considered to be abstract control inputs $\mathbf{c}$.

Figure 5 illustrates the main problem caused by the external coupling of a load to a helicopter (using a rope). The mechanical model of the helicopter is composed of two rigid bodies: the fuselage F and the spinning main rotor MR. The load, denoted as mass point cm_L, is connected to the helicopter fuselage by means of a rope in the point

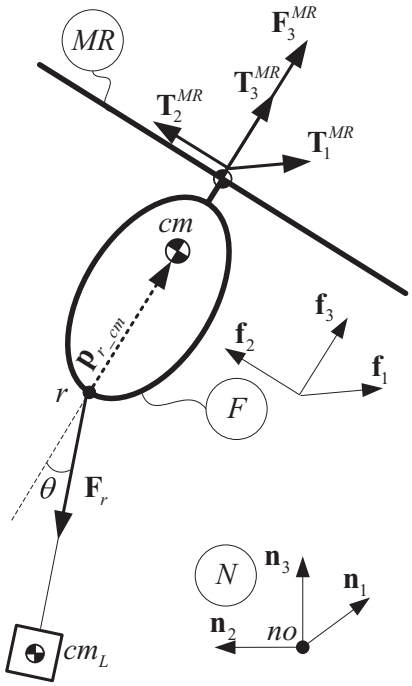

Figure 5. Mechanical model of the helicopter connected to the load. It is composed of two rigid bodies: the fuselage F and the spinning main rotor MR. For a real system it is difficult to place the point r at the helicopter CoM (cm), which causes the connecting vector $\mathbf{p}_{r\text{-cm}}$ to be nonzero.

r. The motion of the whole system is considered with respect to a Newtonian frame N. The point cm is the center of mass (CoM) of the complete helicopter. For a real system it is difficult to place the point r at the helicopter CoM cm, which causes the connecting vector $\mathbf{p}_{r\text{-cm}}$ to be nonzero. Therefore, the rope force $\mathbf{F}_r$ causes a nonzero torque $\mathbf{T}_r = \mathbf{F}_r \times \mathbf{p}_{r\text{-cm}}$ on the helicopter fuselage F. We have shown in Kondak et al. (2006, 2007) that the rotation dynamics of the helicopter modeled as two rigid bodies is complicated but not coupled to the translation dynamics. Therefore, the equations of the rotational dynamics depend only on generalized speeds describing the rotation of the helicopter. The lifting force $\mathbf{F}_3^{\mathrm{MR}}$ generated by the main rotor is always approximately perpendicular to the main rotor plane. This causes the translational accelerations to be completely described by the absolute value of $\mathbf{F}_3^{\mathrm{MR}}$ and the orientation of the helicopter. Therefore, the relationship between rotation and translation dynamics, for a single helicopter, can be expressed as follows: rotation $\Rightarrow$ translation.

However, if one or several helicopters transport a load (each helicopter is connected to the load through one rope), the rope force $\mathbf{F}_r$ and the torque $\mathbf{T}_r$ act on the fuselage of the helicopter. The torque depends on the orientation of the helicopter and its translational motion in the frame N (e.g., if helicopter and load are in free fall, $\mathbf{F}_r$ and $\mathbf{T}_r$ are zero). This creates a more complicated relationship between the rotation and the translation dynamics; for each helicopter: rotation $\Leftrightarrow$ translation.

The translational and rotational motion of one particular helicopter has a direct influence on the dynamics of all other helicopters in the compound, if several helicopters are connected to a common load. Even a translation with constant acceleration, e.g., to the right in Figure 5, can cause oscillation of the angle θ between the rope and the helicopter axis.

The use of an orientation controller that was designed for an uncoupled helicopter is problematic because of the strong mutual coupling between rotation and translation (even if the techniques for robust control design are used). It is noteworthy that in many practical cases the absolute value of the torque $\mathbf{T}_r$ is similar to or even larger than the values of torque needed to control the rotation of an uncoupled helicopter.

For the modeling we consider the general case, in which n helicopters are connected to one common load. To derive the dynamic equations of motion we used the Kane method, see e.g., Kane and Levinson (1985), which allows us to generate the equations for systems with an arbitrary number of helicopters. The coupling between helicopters and load is established by introducing one motion constraint (the rope length is constant over time) for each helicopter in the compound. The resulting equations are used for control design as well as for simulation. For more details on the modeling see Kondak et al. (2007) and Bernard and Kondak (2010). Currently the aerodynamics of the load and the ropes are neglected, but in future work, especially for flights with high velocity, they will be considered.

3.2. Rope Modeling

Two assumptions have been made implicitly regarding the coupling between helicopter(s) and payload during the modeling: The ropes are rigid and massless and the load transportation device (LTD), required for the estimation of the load position, has no influence on the measurement itself. However, several real-flight experiments have demonstrated that these assumptions are not always valid. Assuming normal flight conditions, the ropes are tautened between helicopter(s) and the payload, similar to a string of a musical instrument. Therefore, external disturbances (e.g., wind gusts) or high accelerations can stimulate a natural oscillation of the ropes. We have observed this behavior in real-flight experiments several times. The load motion calculated from angle encoders during these oscillations does not correspond to the real movement of the load. The oscillating angles lead to strong responses from the controller and in the worst case to further excitation of the oscillations. To analyze these effects, the behavior of LTD, rope, and payload was studied in theory and in practical experiments. First, a model composed of LTD, rope, and payload

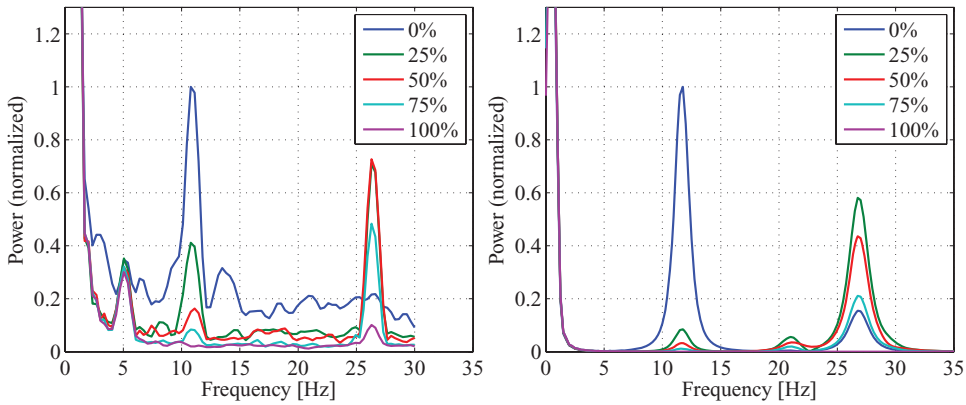

Figure 6. Comparison of simulated (right) and measured (left, load mass 3.0 kg) rope oscillation. The data have been fast Fourier transformed in order to identify the different oscillation frequencies. The color of the lines denotes the position of the points where the data were recorded/simulated: blue line, LTD (0%); green/red/cyan lines, 25%, 50%, and 75% of the rope length; purple line, at the load (100%).

was developed and validated in laboratory experiments. Then the model was used to predict the system behavior for different system parameters. The model consists of a series of 20 interconnected pendulums, in which the links connecting the mass points are considered to be rigid and massless. The topmost pendulum models the LTD, and the parameters (link length, mass) were chosen to reflect the physical properties of the LTD. Similarly, the payload is described by the bottommost mass point and the mass points between LTD and load constitute the flexible rope.

The theoretical model was verified in indoor experiments using a pendulum composed of the LTD, a 0.9-m rope, and loads of 1.5, 3.0, and 4.5 kg. The pendulum was stimulated several times, and the resulting oscillation was recorded by the LTD sensors and a vision system. The vision system measured the motion of the LTD and the load, as well as the rope motion at 25%, 50%, and 75% of the rope length. Figure 6 shows recorded experimental (left, load mass 3.0 kg) and simulation data (right). As can be seen, experiments and simulation match closely and three frequency peaks can be identified in the figure:

First, the pendulum frequency can be calculated (approximated) for the stationary mounting point (high helicopter/payload ratios) to be

$$\mathrm{f}_{\mathrm{pend}} = 1/\left(2\pi\sqrt{l/g}\right) = 1/\left(2\pi\sqrt{0.9/9.81}\right) \cong 0.52 \text{ Hz},$$

where l describes the rope length and g the gravitational acceleration. The actual frequency peak is not visible in the figure, because it was truncated during normalization of the power spectrum. Second, the rope fundamental eigenfrequency is approximated using the theory of sound. The eigenfrequencies of oscillating strings (e.g., a harp string) are calculated only from tension F_t, mass μ, and length of the string l:

$$\mathrm{f}_{\mathrm{rope}}(n) = n(\sqrt{F_t/\mu})/(2\,l),$$

where for $n = 1$ the fundamental eigenfrequency and for $n \geq 2$ the n'th harmonic of the fundamental eigenfrequency are calculated. Assuming a load of 3.0 kg, a fundamental eigenfrequency of 27.4 Hz is estimated. Third, the peak in the middle of the figure is a result of the LTD oscillation. The coupling of the LTD to the rope shifts the frequency upward toward the fundamental eigenfrequency of the rope.

Based on model predictions, coinciding with our experiences from real-flight experiments, the following behavior of the system composed of LTD, flexible rope, and load is estimated: With increasing load mass, the rope fundamental eigenfrequency becomes much higher than the bandwidth of the closed-loop system and the helicopter does not respond to the oscillations. However, the rope length has more influence on the rope eigenfrequency than the load mass and therefore for rope lengths of 5/10 m, even for the high load mass of 4.5 kg, the eigenfrequency becomes 6.04/3.02 Hz. The helicopter controller will react to these oscillations, which can yield instabilities in the system (as was observed in experiments). As a solution we propose a model-based load motion observer, which will be presented in Section 3.4.

3.3. Controller Design

The general scheme of the proposed control algorithm for one or several helicopters coupled to a load is composed of two loops: the outer loop for translation control and the inner loop to control the orientation of each helicopter (see Figure 7).

The input of the control scheme in Figure 7 is the desired trajectory $\mathbf{x}^*(t)$ of the helicopters or of the load. The

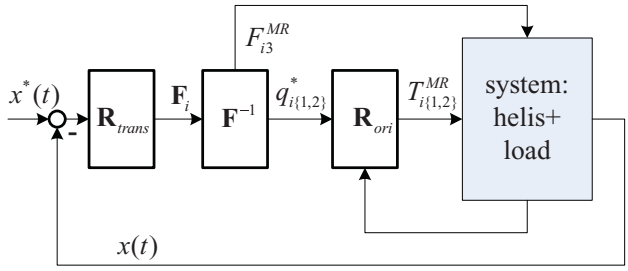

Figure 7. General control scheme for one or several helicopters coupled to a load. The outer loop performs the translation control, and the inner loop controls the orientation of each helicopter.

translational motion of each helicopter is controlled in the outer loop by controller $\mathbf{R}_{\text{trans}}$. Using the deviations from the desired trajectories the controller $\mathbf{R}_{\text{trans}}$ calculates for each helicopter i the forces $\mathbf{F}_i$ that should be generated by its rotors. The helicopter i can realize the force $\mathbf{F}_i$ by adjusting the absolute value of the main rotor lifting force F_{i3}^{MR} and adjusting the orientation of the main rotor plane or fuselage (described by the angles $q^*_{i\{1,2\}}$). The desired orientation of the main rotor plane is controlled in the inner loop by controller $\mathbf{R}_{\text{ori}}$. The values F_{i3}^{MR} and $q^*_{i\{1,2\}}$ are calculated using algebraic relations in block $\mathbf{F}^{-1}$.

As mentioned above, it is usually impossible to attach the rope directly to the CoM of the helicopter. This causes the rope force to create torques, which are imposed on the helicopter fuselage. Therefore, the influence of the coupled system disturbs the helicopter orientation and makes the orientation control a challenging task (Kondak et al. 2006, 2007). The developed approach for the control of coupled helicopters is based on the following three ideas:

- The design of the orientation controller (for each helicopter) accounts for the complete dynamics (translational and rotational) of the whole system, all coupled helicopters and the load. This is required due to the strong mutual coupling between translation and rotation of each helicopter and the load.
- The use of the force sensor in the ropes simplifies the design of the orientation controller and makes it robust against variations of system parameters and disturbances.
- The design of the translation controller is based on the simplified model and accounts only for the translational dynamics of the whole system. In this simplified model the helicopters and the load are modeled as mass points. The model allows the application of arbitrary forces on each mass point, which represents a helicopter. However, the generation of these forces is subjected to a linear dynamic model, which reflects the force generation process of the helicopters.

The utilization of a force sensor in the rope is a key element of the proposed controller design. The measured rope force is easily recalculated into resultant torques acting on the helicopter fuselage. These torques are used in the feedback loop of the orientation controller. The use of the force sensor signal in the feedback loop has three main advantages:

1. The closed-loop system becomes very robust against variation of system parameters and disturbances.
2. The orientation controller design is simplified.
3. The orientation controller does not depend on the number of helicopters connected to the load.

As shown in Kondak et al. (2007), the rotation dynamics of a uncoupled helicopter modeled by rigid bodies for fuselage and main rotor are approximated by the following equations:

$$T_1^{\text{MR}} + K_{12}u_2 + K_{11}\dot{u}_1 = 0, \tag{1}$$

$$T_2^{\text{MR}} + K_{21}u_1 + K_{22}\dot{u}_2 = 0, \tag{2}$$

where $T_{1,2}^{\text{MR}}$ are the torques generated around the longitudinal and lateral axes of the fuselage, $u_{1,2}$ are rotation speeds of the fuselage, and the coefficients K_{xx} are constant parameters of the helicopter and of the main rotor speed. We assume that the influence of the rotation around the vertical axis (rotation speed u_3) on $u_{1,2}$ is small and can be considered as disturbance. This assumption is valid if u_3 is kept close to zero or on constant values. This is achieved by an additional tail rotor controller, with a much smaller time constant than the time constant of the orientation controller for $u_{1,2}$. Equations (1) and (2) are coupled through $u_{1,2}$. This coupling leads to high-frequency oscillations (for the parameters of a typical small-size helicopter) once the system has been stimulated. The control scheme of roll and pitch angles $q_{1,2}$ for an uncoupled helicopter is shown in Figure 8. The blocks shown against a gray background denote the model of the helicopter. The rotation kinematics are represented by block $\mathbf{Q}$, and the rotation dynamics, described by Eqs. (1) and (2), are represented by block $\mathbf{W}$. The controller is composed of blocks $\mathbf{Q}^{-1}$, $\mathbf{D}$ and two feedback loops with gains K_u, K_q for rotation speeds $u_{1,2}$ and orientation angles $q_{1,2}$, respectively. Desired rotational rates are calculated from the angular errors $e_{1,2}$ (interpreted as required Euler angle rates), using controller block $\mathbf{Q}^{-1}$ of the inverse rotation kinematics. Block $\mathbf{D}$ of the controller is used to decouple the plant between $T_{1,2}^{\text{MR}}$ and $u_{1,2}$. The decoupling can be performed by means of known techniques from linear control theory, e.g., using a matrix composed of compensating transfer functions. This orientation controller shows good performance and robustness in simulation and real-flight experiments for different types of helicopters, as described in Kondak et al. (2006, 2007).

As discussed above, the motion of the whole system has a strong influence on the rotational dynamics of the

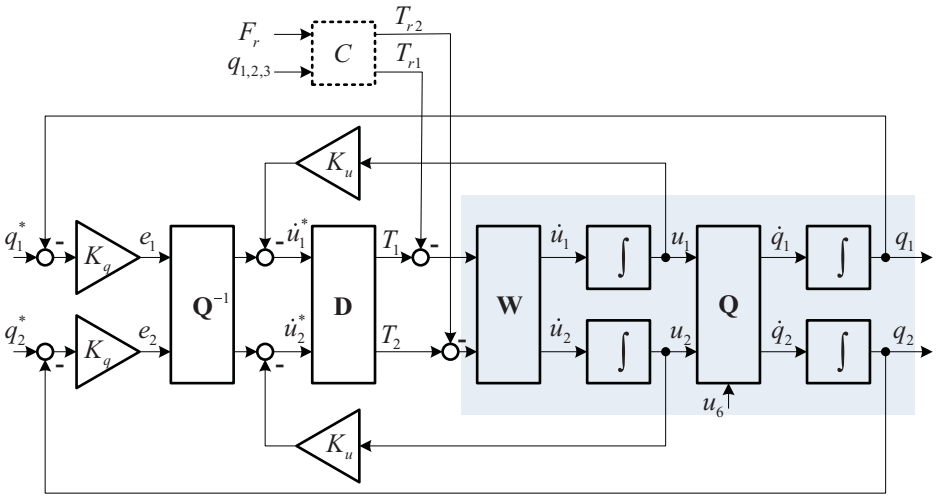

Figure 8. Scheme for the orientation control. The resulting controller is composed of the orientation controller for an uncoupled helicopter and compensator block **C**.

coupled helicopters. To account for this influence, block **D** should be replaced by the inverse rotational dynamics $\tilde{\mathbf{D}}$ not of a single helicopter, but of the whole system (considering both the rotation and translation of each helicopter). Utilizing this new block $\tilde{\mathbf{D}}$, the orientation controller for a helicopter coupled to a load shows performance equal to that of the orientation controller with block **D** for an uncoupled helicopter, considering nominal values of all system parameters ρ_i.

It was shown in simulation that the orientation controller based on inversion block $\tilde{\mathbf{D}}$ for a coupled helicopter (unlike block **D** for a uncoupled helicopter) is quite sensitive to variation of the system parameters ρ_i (5% variation could be critical). To overcome this problem, we propose to use a force sensor in the rope. The measured rope force $\mathbf{F}_r$ is used to calculate the influence of the coupled system on the rotational dynamics of the helicopters. This influence is expressed by the torque $\mathbf{T}_r = \mathbf{F}_r \times \mathbf{p}_r\text{-cm}$, where $\mathbf{p}_r\text{-cm}$ is the position vector, connecting the rope attachment point r and the helicopter CoM. The resulting orientation controller is composed of the orientation controller for an uncoupled helicopter and a compensator block **C** (see Figure 8). The block estimates the disturbance torques T_{r1}, T_{r2} and subtracts them from the torques calculated by the orientation controller. The use of the compensator **C** allows us to decouple the orientation control for each helicopter from the rest of the system. This makes the use of the same orientation controller, independent of the number of coupled helicopters, possible.

There are two reasons for the robustness of the proposed orientation controller: First, the compensation is independent of the mass of the load and the length of the rope, because the actual influence of the load on the fuselage is measured through $\mathbf{F}_r$. Second, as long as the orientation of the helicopter is known, the calculated compensation torque is always in the correct phase.

The details of the presented control algorithms can be found in Bernard and Kondak (2009, 2010) and Kondak et al. (2006, 2007).

3.4. Load Motion Observer

Oscillations of the LTD and rope disturb the motion estimation of the load, as explained in Section 3.2. Therefore, a direct estimation of the load motion based on the measured LTD angles is not feasible. The expected oscillation frequency of the undisturbed load motion is very low (0.52 Hz assuming a rope length of 0.9 m). Therefore, a very simple solution, the low-pass filtering of the measured angles, was applied. Figure 9 shows an angle measured by the LTD (black line) and the angle after application of a fourth-order Butterworth low-pass filter (gray dashed line, cutoff frequency $f_c = 2$ Hz). The gray line corresponds to the result of an observer and is explained later. The disturbance (between 3 and 5 s) still has strong influence on the filtered angle. Additionally, the filtered angle clearly exhibits a large time delay if it is compared to the measurement.

Therefore, an observer-based estimation has been implemented and tested. First we used a linear observer based on the flexible rope model, described in Section 3.2, with a high number of mass points for the rope approximation. This observer converges quickly to the state of the simulated model (the model is observable), but unfortunately it is very sensitive to parameter variations. Assuming that the rope length differs by 0.1 m or the load mass differs by

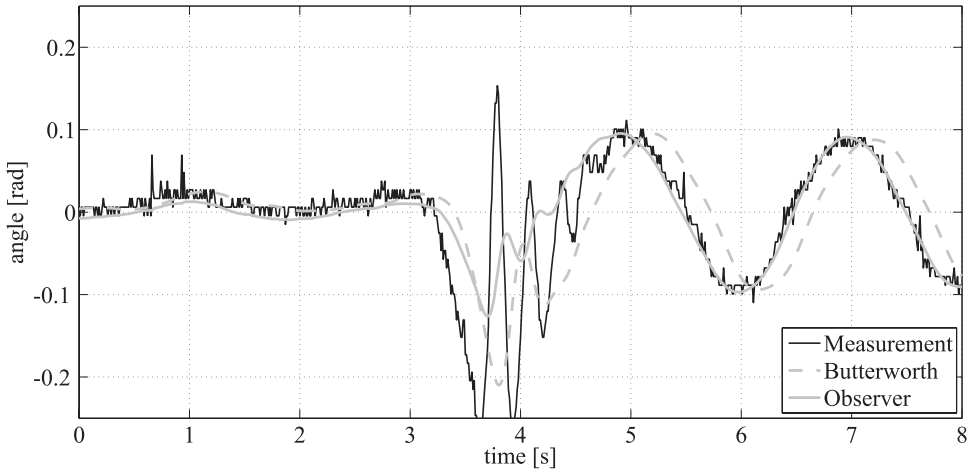

Figure 9. Comparison of simulated and measured rope oscillation. The black line represents an angle measured by the LTD, the gray dashed line is the angle after application of a fourth-order Butterworth low-pass filter (cutoff frequency $f_c = 2$ Hz), and the gray line corresponds to the result of the developed observer.

0.1 kg, the observer is not converging. Therefore, a different approach was tested: The observer was calculated using the simplified model for the controller design. In this model the ropes are simplified to be rigid and massless. The resulting observer is robust against parameter variation and converges quickly to the motion of the undisturbed pendulum. Movements besides the pendulum frequency of 0.52 Hz are effectively filtered out by the observer. Once again Figure 9 is used to compare the performance of the observer to the filter and the direct measurement. The angle estimated by the observer exhibits less sensitivity to the disturbance (between 3 and 5 s) than the filtered angle. Additionally, the observed angle has only a small time delay. In fact, after the observer converged, no time delay was visible compared to the measured angle.

The observer was tested several times in real-flight experiments. Strong, steady winds and wind gusts were present during the experiments and demonstration conducted in May 2009 (see Section 4). Despite these bad environmental conditions several load transportation experiments were conducted successfully. To cross-check its functioning, one experiment was conducted without an observer, using the angles directly measured by the LTD. The experiment needed to be aborted almost immediately because the rope oscillations caused a very strong reaction of the controller. These experiments proved the necessity and the functional efficiency of the observer.

4. VALIDATION IN FIELD EXPERIMENTS

The work presented in this section was conducted within the framework of the AWARE Project[1] funded by the European Commission (June 2006–September 2009). The researchers from the University of Seville led a consortium of five Universities (TUB and the Universities of Seville, Bonn, Stuttgart, and Twente) and three companies (Selex Sensors and Airborne Systems, Flying-Cam, and the Iturri Group) from five European countries.

The general objective of the project was the design, development, and demonstration of a platform composed of heterogeneous systems that are able to operate in a distributed manner in disaster management scenarios without preexisting (or with damaged) infrastructure (Maza, Caballero, Capitan, de Dios, & Ollero, 2011). Thus, the platform comprises self-deployment capabilities (in particular, the autonomous transportation and deployment of different load types, such as small sensors, cameras, and communication equipment) using one or several small-size helicopters. The systems integrated in the platform include aerial robots, wireless sensor networks, ground-fixed-cameras, and ground vehicles with actuation capabilities.

The TUB-H UAVs were used several times in different experiments, with various payloads such as infrared and/or visual cameras, the DD, and the LTD. Configurations with single and multiple UAVs were tested for the transportation and deployment of objects in SAR scenarios. A selection of these field experiments is described in the following.

4.1. Sensor Dropping

During SAR operations the deployment could be required of additional light objects, such as small sensors or communication devices in specific locations around the affected area. Within the framework of the AWARE project, a number of missions involving the deployment of small wireless

[1]http://www.aware-project.net.

(a) One TUB-H autonomous helicopter dropping a sensor

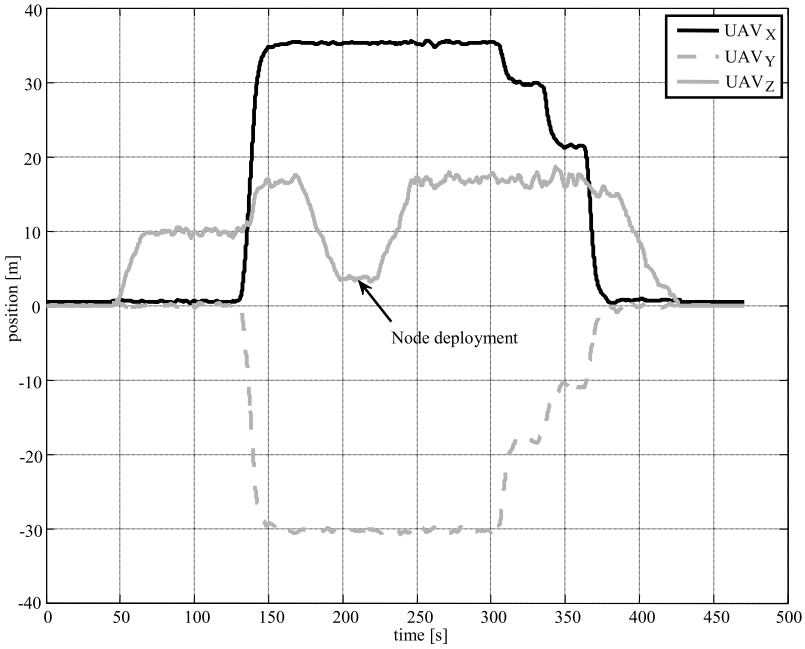

(b) The hovering above the deployment position begins at 160 s and ends at 300 s; during this time span the UAV descends, deploys the node, and ascends again, while maintaining the hovering position in the x/y plane, with a precision of 0.4 m

Figure 10. Sensor-dropping operation by the TUB-H autonomous helicopter equipped with the DD.

sensors were carried out. In Figure 10, the sensor deployment using one TUB-H UAV is shown. The hovering above the deployment position begins at 160 s and ends at 300 s. During this time span the UAV descends, deploys the node, and ascends again, while maintaining the hovering position in the x/y plane, with a precision of 0.4 m. In the z axis a deviation of 1 m was recorded, which is more than twice the deviation of the x and y axes. The reasons were wind gusts of 50 km/h occurring during the flight. In these experiments the gain of the altitude controller was reduced in order to reduce mechanical stress on the helicopters flying under such harsh conditions. As a result, the winds gusts are able to lift the helicopter up or push it down about 1 m, until the height controller is able to compensate.

4.2. Slung-Load Transportation Using a Single UAV

The flight data shown in Figure 11 were recorded on 27 May 2009 in Spain. The plot shows a flight step of 5 m and one of 15 m; another step of 30 m was omitted in order to avoid detail loss (caused by the coarse scaling of the axis). For this experiment a single helicopter equipped with the LTD is used. A jerry can, connected to the LTD using a rope, is transported by the helicopter over a distance of 5 and 15 m. The rope was 5 m long, and the weight of jerry can was 1.1 kg. During the experiment, wind gusts of 30 km/h were measured, which introduced repeated displacement of the load.

During the experiment the load position observer was successfully tested. The position of the load is required in order to stabilize the load and is calculated using the angles measured by LTD. During flight, the rope is normally taut between the helicopter fuselage and the load. If animated by external influences (e.g., by wind gusts) the rope begins to oscillate like the string of a musical instrument. The purpose of the load observer is to estimate the position of the load while rejecting oscillations introduced into the rope itself. Two experiments were conducted: the first without the observer, to prove that these rope oscillations occur during real-flight experiments, and the second with the observer, to prove that the load position observer provides a working solution to the problem. Although the first experiment needed to be aborted, due to the strong controller response to the oscillation of the rope, in the second experiment the observer damped the rope oscillations and preserved the motion of the load.

During hovering, wind gusts of 30 km/h led to damped oscillations of the load, with maximum amplitude of 0.5 m. For real-world applications this is a good value, considering the weather conditions. Owing to the bowing of the rope caused by wind, only an approximate estimation of the absolute load position is possible. For example,

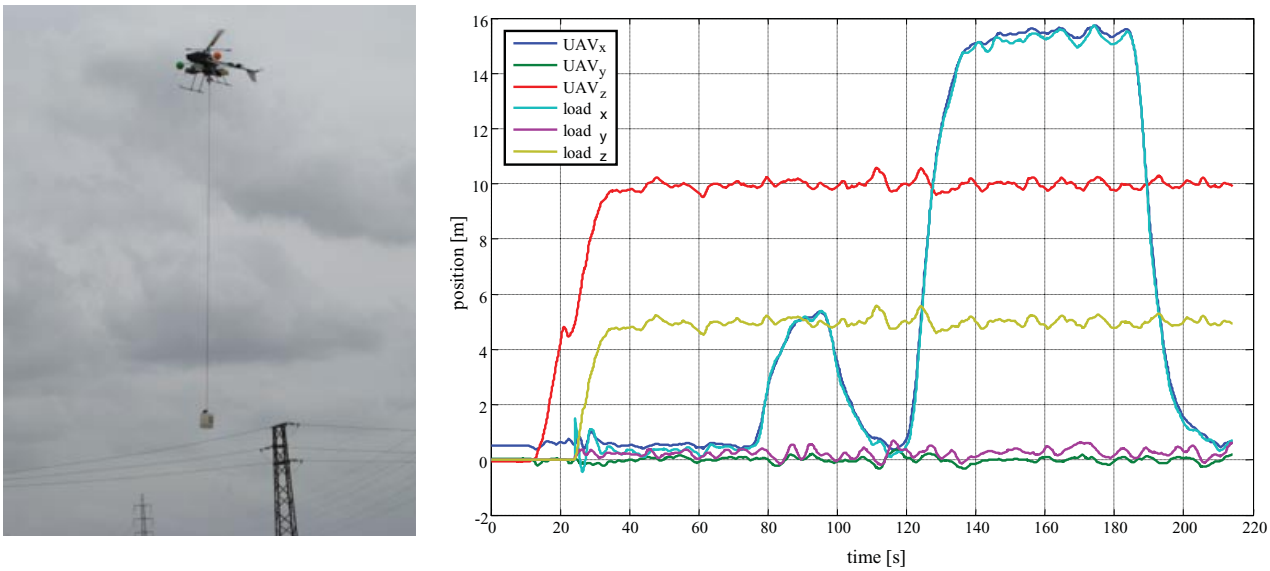

(a) Single TUB-H autonomous helicopter transporting a load

(b) The plot shows a flight step of 5 m and one of 15 m; another step of 30 m was omitted in order to avoid detail loss (caused by the coarse scaling of the axis)

Figure 11. Slung-load transportation using one UAV.

an error of 5 deg, caused by the bowing of the rope, causes a deviation 0.44 m from the real position (for a rope length of 5 m). For real-world applications two solutions exist: first, the use of additional sensors to estimate the position of the load (e.g., vision-based estimation) and second, the manual placement of the load by the UAV operator, in which the operator changes the UAV position step by step until the load is directly above the desired position. The manual placement is favorable whenever the exact GPS position of the placement location is unknown and cannot be measured before takeoff. In that case the helicopter operator uses visual feedback of the deployment process to maneuver the load to the desired position.

4.3. Load Transportation with Multiple UAVs

The first successful experiment was conducted by the authors in Berlin, December 2007.[2] For these flight experiments three identical helicopters as described in Section 2 were used. The helicopters are equipped with a multi-UAV modular autopilot system developed at TUB. The rope is attached to the helicopter by means of the LTD, which is mounted between the landing skids. A load of 4 kg was transported by three helicopters. In this experiment ropes with a length of 13 m were used. The helicopters were arranged as an equilateral triangle on the ground, with a distance of 8 m between them. The coordinates of all three helicopters during the whole flight are shown in Figure 12. The x_{h123} and y_{h123} coordinates describe the horizontal motion of the helicopters, and the z_{h123} coordinates describe the vertical motion. The coordinates of the helicopters are

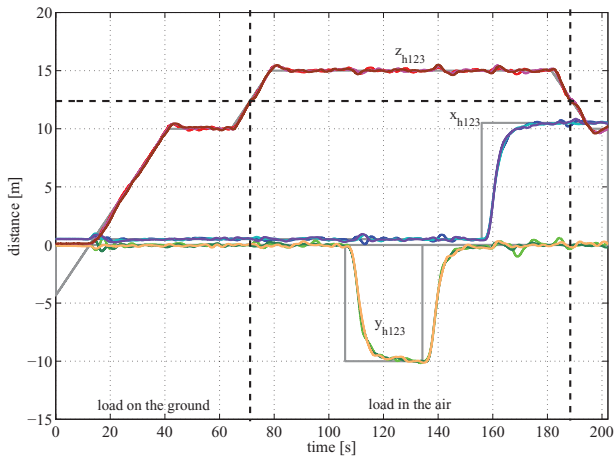

Figure 12. Motion of three helicopters transporting one load of 4 kg. The load was lifted when the helicopters reached approximate 12.4 m. The coordinates of the helicopters are shown in different ground-fixed frames that have the same orientation but different origins (takeoff position of each helicopter); therefore there are no offsets between the helicopter trajectories. The x_{h123} and y_{h123} coordinates describe the horizontal motion of the helicopters, and the z_{h123} coordinates describe the vertical motion.

[2]http://www.youtube.com/watch?v=tl6DYWNe9ac.

shown in different ground-fixed frames that have the same orientation but different origins (takeoff position of each helicopter); therefore there are no offsets between the helicopter trajectories. The mapping of helicopters and line colors is ambiguous. This is acceptable because the motions of the helicopters are discussed together and not individually.

The load was lifted when the helicopters reached approximately 12.4 m. The weight of the load was not considered in the controller, and therefore a small disturbance in the z_{h123} trajectories can be observed at the moment the load was lifted from the ground as well as during strong acceleration in the x, y direction. A position error of each helicopter in hovering was approximately ± 0.3 m. During the whole flight the triangular formation of the helicopters with a precision of about ± 0.3 m and the load was moved very smoothly. To our knowledge these were the very first successful flight experiments to transport a load using multiple autonomous helicopters.

Another experiment was carried out in May 2009 within the scope of the AWARE disaster scenario demonstration: A fire alarm had been declared in a building, and the objective was to place a wireless camera with pan–tilt on the top floor. The camera could provide continuous real-time video to monitor the operations of the firemen and the health status of the victims on the roof of the building. Several coupled helicopters were required for this task because the camera, together with its associated communication equipment and batteries, was too heavy for a single helicopter. To the best of the authors' knowledge, this was the first field experiment involving the transportation of a load from the ground to the roof of a building with three autonomous helicopters. Several videos with the live execution of the mission are included in the online version of this article.

The experiment was executed as follows: The load transportation system (LTS), composed of three TUB-H helicopters and the coupled payload, was ready for operation, and the helicopters were waiting on the three takeoff and landing pads. The platform user specified a load transportation task to deploy the wireless pan–tilt camera on the top floor, and a plan builder module generated the full set of ordered tasks for the LTS.

It should be noted that the enormous complexity of the LTS composed of three helicopters was hidden to the user, who needed only to specify the deployment task by providing the desired GPS location of the load deployment. The altitude specified for the deployment was several meters above the top floor of the building. The autonomous decision-making software of the platform had access to the map of the area in order to plan the deployment task decomposition properly, also taking into account the length of the ropes.

Figure 13 shows a two-dimensional (2-D) view of the trajectories followed by the three TUB-H helicopters and the transported pan–tilt camera unit. The formation of the helicopters was similar to the formation used for the experiment conducted in December 2007: an equilateral triangle, with a distance of 8 m between the helicopters. The weight of the payload composed of camera, transportation

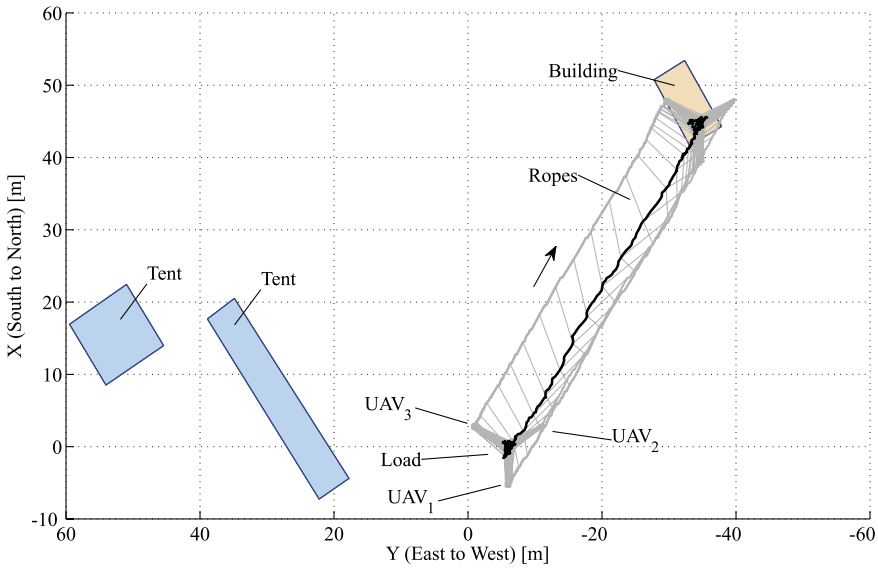

Figure 13. Path followed by the three helicopters transporting the load in the x–y plane. The trajectories of the load and the helicopters are in black and gray, respectively. The arrow indicates the direction of the load transportation. The formation of the helicopters was an equilateral triangle, with a distance of 8 m between the helicopters.

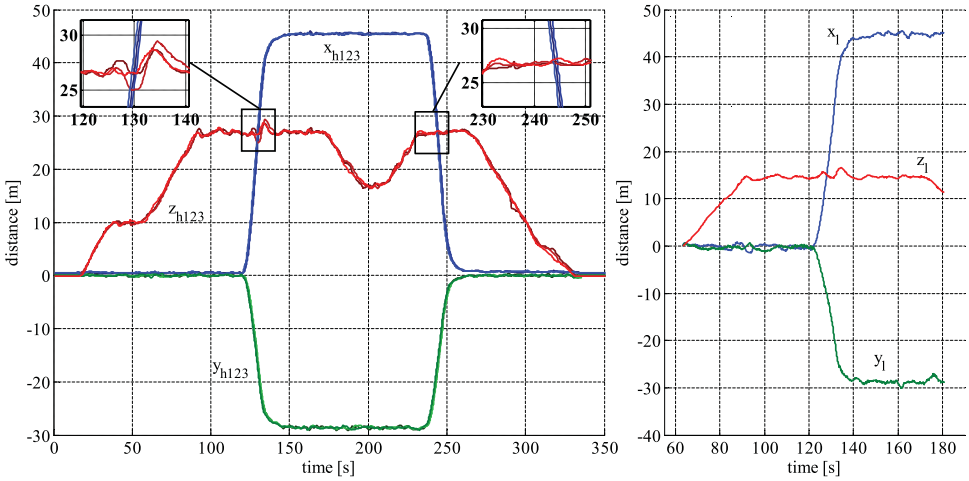

Figure 14. Values of the x, y, and z coordinates of the helicopters (left) and the load (right) during the flight. The coordinates of each helicopter and the load are given relative to one global Newtonian reference frame, but for each helicopter and for the load the coordinates were plotted with respect to a relative origin (the takeoff position of the respective helicopter or the liftoff position of the load). The trajectories of the helicopters show almost no deviation relative to each other.

housing, and batteries was approximately 5 kg. The trajectories of the helicopters are plotted in gray, and the trajectory of the camera is plotted in black. The estimated rope positions are plotted as gray lines, where a time step of 1 s elapsed between two successive estimations. The arrow indicates the direction of the load transportation. It is noteworthy that despite the stormy weather conditions, the load stayed clearly within the extends of the roof during the deployment.

Figure 14 complements the flight data presented in Figure 13, by depicting the values of the x, y, and z coordinates of the helicopters and the load during the flight. The motion of the load is depicted from the moment the load was lifted off the ground to the moment it was deployed on the roof. The coordinates of each helicopter and the load are given relative to one global Newtonian reference frame, but for each helicopter and for the load, the coordinates were plotted with respect to a relative origin (the takeoff position of the respective helicopter or the liftoff position of the load). The mapping of helicopters and line colors is ambiguous, but similar to Figure 12 the motions of the helicopters are only discussed together. The trajectories of the helicopters show almost no deviation relative to each other. Therefore, the helicopters preserved their relative formation during the whole flight. To demonstrate the robustness of the translation controller, the additional weight of the load was neglected during the experiment. Therefore, in the interval [120 s, 140 s] the strong acceleration of the helicopters caused a height deviation. However, besides this deviation no additional side effects were noticeable. During the return flight [240 s, 260 s], after the load deployment, no disturbance of the height is visible. It should be mentioned that during the execution, wind gusts around 35 km/h were registered. Therefore, the performance of the coupled LTS is considered to be very good.

Several photographs of the LTS during the execution of the mission are shown in Figure 15. A fourth helicopter used to acquire airborne video footage of the mission can be seen in two pictures. Finally, Figure 16 contains a screenshot of the human–machine interface application captured during the execution, as well as one image transmitted from the transported camera once it had been deployed on the top of the building.

5. CONCLUSIONS AND LESSONS LEARNED

The experiments conducted within the AWARE demonstration in 2009 imposed high availability requirements on all involved subsystems. For two reasons this was particularly true for the autonomous helicopters: First, the helicopters were the designated platform for the transportation (and deployment) of various sensors and therefore they were involved in almost every experiment. Second, the experiments included the demonstration of the LTS, which requires the simultaneous operability of three helicopters. Therefore, several preventive measures were taken to ensure the successful conduct of the experiments. The complexity of these measures ranged from simple (such as the regular maintenance of the helicopters or the availability of spare parts) to complex (such as the adherence to preflight checks/procedures or the possibility to adapt hard- and software in the field, toward the requirements of the experiment or the actual environmental conditions). In particular,

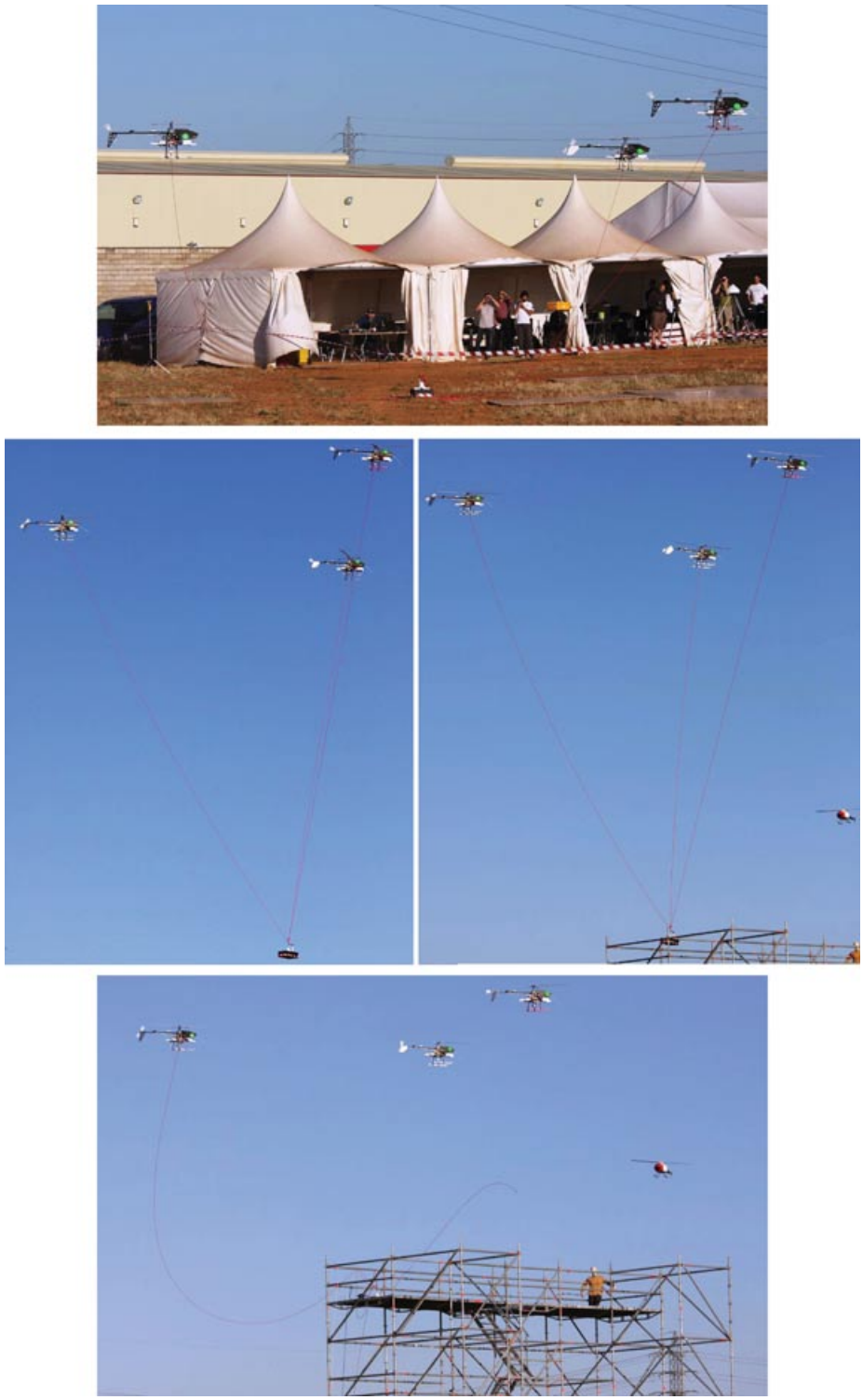

Figure 15. Three UAVs transporting a pan–tilt wireless camera to the roof of a building with a height of 12 m in Utrera (Spain) in May 2009. The images show the mission during the takeoff (top), during the actual load transportation (middle left), shortly before (middle right), and shortly after (bottom) the load deployment. In two pictures a fourth helicopter is visible, which was used to acquire airborne video footage of the mission.

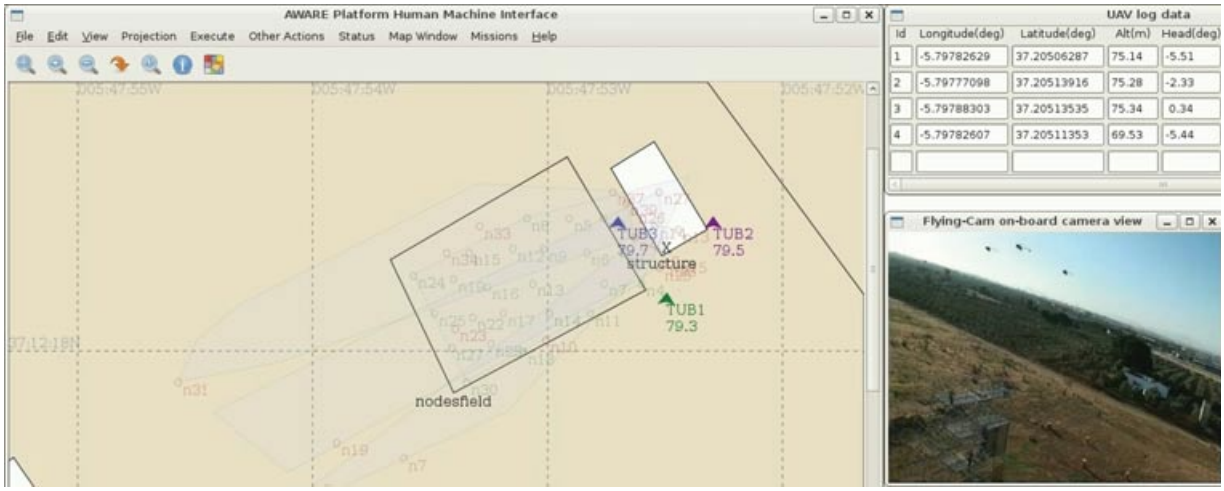

(a) Map of the area with the position and heading of the three LTS helicopters represented by arrows; images transmitted by a fourth helicopter and telemetry from all the UAVs

(b) Camera deployed on the top floor of the building; the operator used the pan–tilt to find one victim; the LTS is still over the deployment location after releasing the ropes

Figure 16. Screenshot of the platform human–machine interface during the execution of the load transportation mission in 2009. The different elements in the interface were (top left) map of the area with the position and heading of the three LTS helicopters represented by arrows; (center) images transmitted by another helicopter and telemetry from all the UAVs; (right) interface to control the transported camera with pan–tilt.

the adaptability of hardware and software has been proven to be useful during the experiments:

The combustion engine of a helicopter exhibited signs of imminent failure during the conduct of an experiment. Therefore, the experiment was aborted immediately and the helicopter was landed safely. Then, in order to proceed with the experiment as quickly as possible, the payload was mounted to a different helicopter. The modular design of the system components, in combination with the strut profile mounting frame (described in Section 2), allowed the quick relocation of the payload to a different helicopter and the resumption of the experiments.

The adverse weather conditions with high wind speeds ($\geq$25 km/h) and strong wind gusts ($\geq$35 km/h), particularly during the last days of the AWARE project experiments, required the adaption of the helicopter controller. It was possible to operate the helicopters during these bad weather conditions, although the controller was optimized for the operation during medium wind speeds ($\leq$20 km/h). The controller was able to quickly compensate

for the displacements of the helicopter (caused by the wind gusts). However, the helicopter was operating close to its performance limit, and the strong reactions of the controller caused unnecessarily high stress on rotors, structure, and engine. Therefore, the control coefficients of the height controller were relaxed, which allowed the helicopter to be lifted up or to be pushed down (±1 m) by the wind gusts. This measure strongly reduced the stress on the helicopter and improved the precision of the remaining two position coordinates. In Section 4.1 an experiment utilizing the modified controller coefficients is described. The controller coefficients were modified online during a single test flight, in which the Matlab/Simulink external mode interface was utilized; see Section 2 for a description of the software system. Without the possibility of online parameter modification, several test flights would have been required until good parameters could be found. Using the Matlab/Simulink interface it was possible to upload different controller coefficients and directly monitor the improvements achieved by a particular set of coefficients. Therefore, only a single flight of approximately 10-min length was required for the adaption of the coefficients, and the schedule of planned experiments was only insignificantly delayed.

The above examples were chosen because they clearly demonstrate the benefits of the excellent system adaptability. However, beside these examples, the importance of the system adaptability was witnessed several times during the field experiments. Therefore it is possible to conclude that adaptability of the system was a key element required for the successful completion of the field experiments.

The paper has presented the multi-UAV LTS, which requires consideration of physical interactions between aerial robots. The multi-UAV architecture developed in the AWARE project allows different levels of interaction among the UAVs and between the UAVs and the environment, including both sensing and actuation. In particular, the paper has presented results obtained in the AWARE project demonstrating the lifting and transportation of a slung load by one helicopter and also by three coupled helicopters, which has been the first demonstration of this challenging application.

The proposed methods open many different new opportunities in missions involving the cooperation of multiple UAVs for applications such as SAR and interventions in disaster management and civil security. The transportation of loads by means of UAVs can be also considered as a first step toward cargo transportation by UAVs or even toward the evacuation of people in SAR operations.

6. APPENDIX: INDEX TO MULTIMEDIA EXTENSIONS

The table shows the different videos of the LTM carried out in 2009 in the framework of the AWARE Project. The videos are available as Supporting Information in the online version of the article.

Extension	Media type	Description
1	Video	Load transportation mission with multiple UAVs (ground camera view)
2	Video	Load transportation mission with multiple UAVs (transported wireless camera view)
3	Video	Load transportation mission with multiple UAVs (human–machine interface view)
4	Video	AWARE project summary (including load transportation)

ACKNOWLEDGMENTS

This work was partially supported by the AWARE Project (IST-2006-33579) funded by the European Commission under FP6 and also by the ROBAIR Project (DPI2008-03847) funded by the Spanish Research and Development Program.

REFERENCES

Arai, M., Tanaka, Y., Hirose, S., Kuwahara, H., & Tsukui, S. (2008). Development of "Souryu-Iv" and "Souryu-V": Serially connected crawler vehicles for in-rubble searching operations. Journal of Field Robotics, 25(1–2), 31–65.

Bernard, M., & Kondak, K. (2009, May). Generic slung load transportation system using small size helicopters. In Proceedings of the IEEE International Conference on Robotics and Automation, Kobe, Japan (pp. 3258–3264).

Bernard, M., & Kondak, K. (2010). Load transportation system based on autonomous small size helicopters. Aeronautical Journal, 114(1152), 191–198.

Birk, A., & Carpin, S. (2006). Rescue robotics—A crucial milestone on the road to autonomous systems. Advanced Robotics Journal, 20(5), 595–695.

Borenstein, J. (2000). The OmniMate: A guidewire- and beacon-free AGV for highly reconfigurable applications. International Journal of Production Research, 38(9), 1993–2010.

Cicolani, L. S., & Kanning, G. (1992). Equations of motion of slung-load systems, including multilift systems (Tech. Rep. NASA TP-3280). NASA Ames Research Center.

Corke, P., Hrabar, S., Peterson, R., Rus, D., Saripalli, S., & Sukhatme, G. (2004a, April/May). Autonomous deployment and repair of a sensor network using an unmanned aerial vehicle. In Proceedings of the IEEE International Conference on Robotics and Automation, New Orleans, LA (pp. 3602–3608).

Corke, P., Hrabar, S., Peterson, R., Rus, D., Saripalli, S., & Sukhatme, G. (2004b, June). Deployment and connectivity repair of a sensor net with a flying robot. In Proceedings

of the 9th International Symposium on Experimental Robotics, Singapore.

Gage, A., Murphy, R., Rasmussen, E., & Minten, M. B. (2004). Shadowbowl 2003: Lessons learned from a reachback exercise with rescue robots. IEEE Robotics & Automation Magazine, 11(3), 62–69.

Goodrich, M. A., Morse, B. S., Gerhardt, D., Cooper, J. L., Quigley, M., Adams, J. A., & Humphrey, C. (2008). Supporting wilderness search and rescue using a camera-equipped mini UAV. Journal of Field Robotics, 25(1–2), 89–110.

Hollinger, G., Singh, S., Djugash, J., & Kehagias, A. (2009). Efficient multi-robot search for a moving target. International Journal of Robotics Research, 28(2), 201–219.

Hsieh, M. A., Chaimowicz, L., Cowley, A., Grocholsky, B., Keller, J. F., Kumar, V., Taylor, C. J., Endo, Y., Arkin, R. C., Jung, B., Wolf, D. F., Sukhatme, G., & MacKenzie, D. C. (2007). Adaptive teams of autonomous aerial and ground robots for situational awareness. Journal of Field Robotics, 24(11), 991–1014.

Hsieh, M. A., Cowley, A., Kumar, V., & Taylor, C. J. (2008). Maintaining network connectivity and performance in robot teams. Journal of Field Robotics, 25(1–2), 111–131.

Huntsberger, T. L., Trebi-Ollennu, A., Aghazarian, H., Schenker, P. S., Pirjanian, P., & Nayar, H. D. (2004). Distributed control of multi-robot systems engaged in tightly coupled tasks. Autonomous Robots, 17(1), 79–92.

Johnson, W. (1980). Helicopter theory. Mineola, NY: Dover Publications.

Kane, T., & Levinson, D. (1985). Dynamics: Theory and applications. New York: McGraw-Hill.

Kondak, K., Bernard, M., Losse, N., & Hommel, G. (2006, May). Elaborated modeling and control for autonomous small size helicopters. In ISR/ROBOTIK 2006 Joint Conference on Robotics, Munich, Germany.

Kondak, K., Bernard, M., Meyer, N., & Hommel, G. (2007, April). Autonomously flying VTOL-robots: Modeling and control. In Proceedings of the IEEE International Conference on Robotics and Automation, Rome, Italy (pp. 2375–2380).

Kosuge, K., & Sato, M. (1999, October). Transportation of a single object by multiple decentralized-controlled nonholonomic mobile robots. In Proceedings of the IEEE International Conference on Intelligent Robots and Systems, Kyongju, Korea (vol. 3, pp. 1681–1686).

Maza, I., Caballero, F., Capitan, J., de Dios, J. M., & Ollero, A. (2011). A distributed architecture for a robotic platform with aerial sensor transportation and self-deployment capabilities. Journal of Field Robotics, 28(3), 303–328.

Michael, N., Fink, J., & Kumar, V. (2010). Cooperative manipulation and transportation with aerial robots. Autonomous Robots, 30(1), 73–86.

Micire, M. J. (2008). Evolution and field performance of a rescue robot. Journal of Field Robotics, 25(1–2), 17–30.

Mittal, M., Prasad, J. V. R., & Schrage, D. P. (1991). Nonlinear adaptive control of a twin lift helicopter system. IEEE Control Systems Magazine, 11(3), 39–45.

Murphy, R., Tadokoro, S., Nardi, D., Jacoff, A., Fiorini, P., Choset, H., & Erkmen, A. (2008). Search and rescue robotics. In Springer Handbook of Robotics (pp. 1151–1173). Berlin: Springer Verlag.

Murphy, R. R., & Stover, S. (2008). Rescue robots for mudslides: A descriptive study of the 2005 La Conchita mudslide response. Journal of Field Robotics, 25(1–2), 3–16.

Poppinga, J., Birk, A., & Pathak, K. (2008). Hough based terrain classification for realtime detection of drivable ground. Journal of Field Robotics, 25(1–2), 67–88.

Reynolds, H. K., & Rodriguez, A. A. (1992). H_∞ control of a twin lift helicopter system. In Proceedings of the 31st IEEE Conference on Decision and Control, Tucson, AZ (pp. 2442–2447).

Sugar, T., & Kumar, V. (1998). Decentralized control of cooperating mobile manipulators. In Proceedings of the IEEE International Conference on Robotics and Automation, Leuven, Belgium (vol. 4, pp. 2916–2921).

Wagtendonk, W. (2006). Principles of helicopter flight. New Castle, WA: Aviation Supplies & Academics.